RESEARCH ARTICLE

Check for updates

Linking triptycene to silole: a fruitful association†‡

Kassem Amro,[a] Anil K. Thakur,[b] Marc Rolland,[c] Arie Van Der Lee, [iD][c] Vincent Lemaur, [iD][d] Roberto Lazzaroni, [iD][d] Joëlle Rault-Berthelot,[e] Cyril Poriel, [iD][e] Lionel Hirsch, [iD][b] Sébastien Clément*[a] and Philippe Gerbier [iD]*[a]

1,1′-Disubstituted-2,3,4,5-tetraphenylsiloles incorporating triptycene moieties **Tp-DMTPS** and **Tp-MPTPS** were prepared and characterized. Like other 2,3,4,5-tetraphenylsiloles, both compounds exhibit aggregation-induced emission (AIE) behavior. Unexpectedly, the solid state PL emission of **Tp-DMTPS** show dependence according to the degree of crystallinity of the powders. While precipitates display a blue-green emission, microcrystalline powders emit in the yellow-orange region. Moreover a rare reversible mechanohypsochromic phenomenom is observed: upon grinding, the emission of a micro-crystalline powder changes from yellow-orange to blue-green, the original emission being restored by annealing the sample. The mechanism of this blue-shift upon crystal grinding was investigated by X-ray diffraction, ^{13}C CP-MAS NMR and DFT calculations. Under mechanical stress, strong intermolecular CH/π interactions are found to promote the less energetically stable population of conformers present in the crystals, leading to this blue-shift. Finally the influence of the triptycene moieties on the thermal and structural stability of **Tp-DMTPS** and **Tp-MPTPS** was studied. Compared with **DMTPS** and **MPTPS** parents, a general enhancement of the properties is noticed, especially when used as active layer in OLED fabrication. Our results suggest that the attachment of triptycene moieties to π-conjugated molecules is an interesting way to improve their thermal, structural and photophysical properties for sensing or optoelectronic applications.

Introduction

Limited to very few applications for a long time because of their complicated synthetic chemistry,[1] siloles or silacyclopentadienes experienced a spectacular rebirth thanks to the works of K. Tamao and S. Yamaguchi in the late 90s.[2,3] Indeed, the general and versatile synthesis *via* an intramolecular reductive cyclization of diethynylsilanes they proposed allowed the preparation of various 2,5-difunctional siloles that would be otherwise very difficult to obtain. Shortly afterwards, on account of their unique electronic properties, *i.e.*, their very low LUMO energy levels combined with high fluorescence quantum yields in the solid state, siloles were used successfully as both emissive and electron-transporting materials in organic light emitting diodes (OLED) manufacture.[4–7] The origin of their electronic properties is the consequence of an efficient interaction between the σ* orbital of the silole silicon atom with the π* orbital of the butadiene fragment[5,8] whereas the origin of their outstanding high solid-state fluorescence is attributed to the aggregation induced emission (AIE) phenomenon that was described for the first time with 1-methyl-1,2,3,4,5-pentaphenylsilole.[9] Since then, AIE materials are the subject of intense scientific research and have found many applications that encompass various domains going from organic electronics to theranostic bioprobes.[10–14] Moreover, with the growing number of AIE materials described in the literature, rather new and uncommon phenomena such as reversible mechanofluorochromism have started to be reported since their first observation with tetraphenylethene (TPE) and diphenyldibenzofulvene (DPDBF) derivatives.[15–20]

In small molecules-based organic electronics, besides the device efficiency, the thermal and structural stabilities of the used organic materials are an important concern.[21,22] Indeed, for instance, an operating OLED releases heat that may alter

[a] *Institut Charles Gerhardt de Montpellier (ICGM, UMR 5253), Université de Montpellier, CNRS, ENSCM, F-34095 Montpellier, France.*
 E-mail: philippe.gerbier@umontpellier.fr, sebastien.clement1@umontpellier.fr
[b] *Institut Européen des Membranes (IEM, UMR 5635), Université de Montpellier, CNRS, ENSCM, F-34095 Montpellier, France*
[c] *Laboratoire de l'Intégration du Matériau au Système (IMS, UMR 5218), Université de Bordeaux, CNRS, Bordeaux INP, ENSCBP, 33405 Talence, France*
[d] *Laboratoire de Chimie des Matériaux Nouveaux, Institut de Recherche sur les Matériaux, Université de Mons (UMONS), 7000 Mons, Belgium*
[e] *Institut des Sciences Chimiques de Rennes, (ISCR, UMR 6226), Université de Rennes, CNRS, F-35000 Rennes, France*

† Dedicated to Profs J. Veciana and C. Rovira at the occasion of their 70th anniversary.
‡ Electronic supplementary information (ESI) available. CCDC 1963525 and 1963526. For ESI and crystallographic data in CIF or other electronic format see DOI: 10.1039/d0qm00087f

Fig. 1 Labelling scheme for **Tp-DMTPS** ($R1' = Me$) and **Tp-MPTPS** ($R1' = Ph$).

Scheme 1 Synthetic route to **Tp-DMTPS** and **Tp-MPTPS** (see more details in ESI‡).

quickly its efficiency.[23] This is the reason why materials with high melting points and high glass transition temperatures (T_g) are desirable to achieve the fabrication of devices with good durability. One of the strategies used to increase the thermal stability of the organic layers is to crosslink the adequately functionalized molecules after their deposition.[24] Another strategy involves the control of the spatial organization, *i.e.*, distance and relative orientation of the constitutive molecules through the chemical synthesis and/or the use of an appropriate construction scaffold.[25] Triptycene with its fascinating paddle-wheel shape has been widely used for this purpose in supra-molecular chemistry, polymer chemistry and materials science.[26–28] However, in spite of the thermal stabilization afforded by its presence in the molecular structures, only few examples of the use triptycene-based luminescent materials in OLEDs have been reported so far.[29–31]

With this in mind we report herein the synthesis and structural characterization of two novel silole derivatives incorporating triptycene moieties at the 2,5-positions (**Tp-DMTPS** and **Tp-MPTPS**, Fig. 1) with the first aim to use them as emissive layers in OLEDs. We will focus on the interplay between the triptycene side-groups and the silole core that induces an original behavior in terms of thermal and structural stability, luminescence and mechanofluorohypsochromism, phenomenon that was still rarely observed up to now.[32–37] We show that the modulation of the structure in the solid state resulting from the incorporation of triptycene groups affords an enhancement of OLED performance by formation of morphologically stable non-crystalline emissive layers.

Results and discussion

Synthesis

The siloles **Tp-DMTPS** and **Tp-MPTPS** were conveniently prepared by the method previously described by Tamao *et al.* that involves the intramolecular reductive cyclization of 1,1-bis(phenyl-ethynyl)silane, followed by a palladium-catalyzed cross-coupling reaction with the appropriate bromoaryl compound (Scheme 1).[4,38] 9-(*p*-Bromophenyltriptycene) was prepared *via* a Diels–Alder reaction between *in situ* generated benzyne, and 4'-bromo-phenylanthracene.[39] **Tp-DMTPS** and **Tp-MPTPS** were isolated in 54 and 49% yields, respectively, as pale yellow powders.
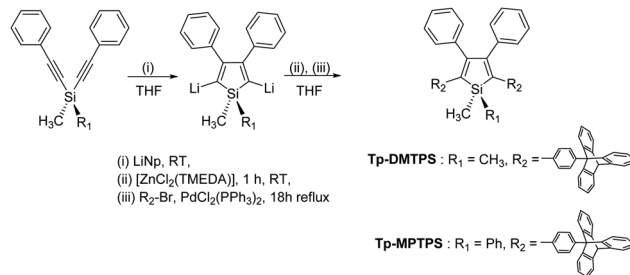
Crystal structure

As shown in Fig. 2 (and Fig. S3–S6, ESI‡), the molecular packing of **Tp-DMTPS** is mainly governed by the paving of the triptycene moieties in alternating up (one of the phenyl ring parallel to the *c*-axis) and down (antiparallel to the *c*-axis) columns leading to a layered structure. Inside the triptycene double layer, the 3,4-diphenylsilole moieties also adopt an up and down columnar packing corresponding to the orientation of the triptycene side-groups. Interestingly, the structure shows that the silole rings could be inclined either on the right or on the left with respect to a plane going through the middle of a column (Fig. 3). This situation leads to the co-existence of two conformers in the crystal, which will be named *R* and *L*. In the *R*-conformer, the methyl group C69 (see Fig. 3) is nestled between two phenyl

Fig. 2 Views of the crystal packing of **Tp-DMTPS** showing the triptycene paving in the *bc* plane for (a) *R*-conformers and (b) *L*-conformers.
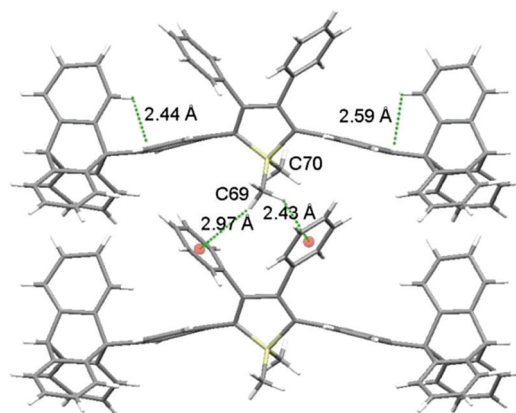

Fig. 3 View of the *R*-conformers of **Tp-DMTPS** in the *ab* plane showing the methyl C69 nestling between the aromatic rings. Intra and inter-molecular CH/π interactions are marked with green dotted lines.

This journal is © The Royal Society of Chemistry and the Chinese Chemical Society 2020

Mater. Chem. Front., 2020, **4**, 2006–2017 | **2007**

rings of the molecule immediately below. Short CH/π hydrogen bonds are present between two hydrogen atoms belonging to the methyl group and the interacting phenyl rings ($d_{CH/\pi}$ = 2.43 Å and 2.97 Å).[40] In the *L*-conformer (Fig. S5 and S6, ESI‡), the other methyl group C70 is nestled between the phenyl rings and shorter CH/π hydrogen bonds are observed ($d_{CH/\pi}$ = 2.55 Å and 2.85 Å).

The distance and the orientation of the CH/π hydrogen bonds observed in each conformer are in the range of what is frequently observed in the literature ($d_{CH/\pi}$ = 2.73 ± 0.13 Å).[40] Since it is only the 1,1-dimethyl-3,4-diphenylsilole moiety that is involved in this swinging, this induces torsion angle modifications between the silole core and the four phenyl rings at its periphery (Table 1). The phenyl rings located at the 2,5-position of the silole core are locked within the structure because of a strong CH/π interaction between their aromatic system and a hydrogen atom belonging to the triptycene moieties ($d_{CH/\pi}$ = 2.44 Å and 2.59 Å). This CH/π interaction leads to a moderate bending of the phenyl moiety with respect to the threefold axis of the triptycene by *ca.* 17° (a bending angle of 6° is found in the crystal structure of 9-phenyltriptycene[41]). If present in solution, this strong CH/π interaction should lead to an appreciable shift of the ¹H NMR signal of the corresponding hydrogen atom compared to the two other ones, because of the shielding anisotropy cones of the adjacent phenyl ring.[42] However in none of the molecules incorporating triptycene moieties we have synthesized (see Fig. S30–S32, ESI‡), this feature was observed. In every cases, the hydrogen atoms of the C(2) carbon atoms (see Fig. 1 for labelling) belonging to the triptycene paddlewheels are equivalents, indicating a free rotation of the later in solution at ambient temperature.

The crystal packing of **Tp-MPTPS** (Fig. S7, ESI‡) does not show any of the features found with **Tp-DMTPS**. Probably because of the presence of a phenyl ring attached to the silicon atom, the triptycene moieties are not able to organize themselves in regular layers. Consequently, the molecular packing is less dense in **Tp-MPTPS** and CH₂Cl₂ molecules are found in the structural voids. Notably short CCl/π halogen interactions are also observed between one chlorine atom belonging to these molecules and one of the phenyl rings adjacent to the silole ring ($d_{CCl/\pi}$ = 3.51 Å, see Fig. S2, ESI‡).[43] Because of the chirality of the silicon atom in **Tp-MPTPS**, both (*R*) and (*S*) enantiomers were found in the crystal lattice. The molecular structure of **Tp-DMTPS** shows a paddlewheel arrangement of the 2, 3, 4 and 5-phenyl rings around the
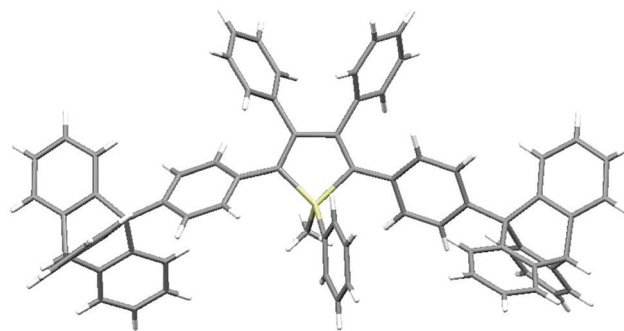

Fig. 4 View of **Tp-MPTPS** molecular structure.

silole core, whereas a more conventional propeller-like disposition of the phenyl rings is found in **Tp-MPTPS** (Fig. 4). In this case, the structure also reveals that the phenyl moieties are bent off the threefold axis of the triptycene by angle of 16° on average.

Hirshfeld surface analysis

The Hirshfeld surfaces[44] of both conformers of **Tp-DMTPS** (Fig. 5) were calculated with the CrystalExplorer program[45] and are mapped with the d_{norm} property[46] where the color scheme goes from red (d_{norm} = −0.2664 and −0.2795 for conformers *L*- and *R*-, respectively) to blue (d_{norm} = 2.2715 and 2.2586 for conformers *L*- and *R*-, respectively). The most notable interactions shown in red in Fig. 5 are indeed in both cases between the methyl hydrogens and the aromatic rings of adjacent molecules. Interestingly, in *R*-conformer, the secondary interactions between the CH systems of one ring to the π-system of an adjacent ring seem to be less important than in *L*-conformer. An analysis of the elemental fingerprint plots shows that the relative contributions of the different interactions in the two conformers are anyhow approximately equal: 31.7%/31.3% for H···C/C···H interactions and 64.8/65.2% for hydrophobic H···H interactions. The Hirshfeld surface analysis of **Tp-MPTPS** (Fig. S8, ESI‡) shows d_{norm} ranging from −0.1149 to 2.3526 with

Table 1 Selected torsion angles and calculated orbital energies of **Tp-DMTPS** and **Tp-MPTPS**

		φ_2 (°)	φ_3 (°)	φ_4 (°)	φ_5 (°)	HOMO (eV)	LUMO (eV)	E_g (eV)
Tp-DMTPS	Optimized[a]	42.6	59.5	58.2	42.6	−5.56	−1.99	3.57
	R-conformer[b]	54.0	70.2	50.4	58.6	−5.65	−1.81	3.84
	L-conformer[b]	74.2	76.0	71.4	67.5	−5.88	−1.64	4.24
Tp-MPTPS	Optimized[a]	43.9	59.4	58.1	43.6	−5.58	−2.00	3.58
	X-ray	51.4	53.6	56.2	33.1			

[a] B3LYP/6-31G optimization. [b] Determined from XRD data.

Fig. 5 Hirshfeld surfaces for the *L*-conformer (top) and the *R*-conformer (bottom) of **Tp-DMTPS**.

2008 | *Mater. Chem. Front.*, 2020, **4**, 2006–2017

This journal is © The Royal Society of Chemistry and the Chinese Chemical Society 2020

the following relative elemental interactions: H···H (62.4%), H···C (31.5%), H···Cl (3.6%) and C···Cl (0.7%). However, it is clearly seen that the intermolecular interactions in the case of **Tp-MPTPS** are more dispersive than in the case of **Tp-DMTPS**.

Thermal properties

The thermal properties of **Tp-DMTPS** and **Tp-MPTPS** were examined by thermogravimetric analysis (TGA) and differential scanning calorimetry (DSC) measurements. As shown in Fig. 6, the TGA of **Tp-DMTPS** exhibits a weight loss in one step leading to a high decomposition temperature (T_d) of 486 °C. In contrast, the weight loss of **Tp-MPTPS** takes place in two steps. The first weight loss of *ca.* 10% could be ascribed to the loss of interstitial solvent molecules, as observed in the crystal structure of **Tp-MPTPS** (see above). This high temperature of desolvation may be due to the strong CCl/π halogen interactions that have been characterized in the crystal lattice. The second weight loss is due to the decomposition of **Tp-MPTPS** molecule. As for **Tp-DMTPS**, a high T_d of 489 °C was noticed highlighting the high thermal stability of these two siloles. It is noteworthy that these T_d are higher than their parent compounds, namely, 1,1-dimethyl-2,3,4,5-tetraphenylsilole (**DMTPS**): 272 °C and 1-methyl-1,2,3,4,5-pentaphenylsilole (**MPTPS**): 309 °C.[47] The same trend is observed with the melting point, measured at 431 °C for **Tp-DMTPS**; 250 °C above that of the **DMTPS** parent (Fig. S13, ESI‡).[47]

Photophysical properties

The UV-visible absorption and fluorescence spectra were measured in dilute dichloromethane solution (Fig. 7). The data are gathered in Table 2. **Tp-DMTPS** exhibits an absorption maximum at 357 nm corresponding to the π–π* transition involving mainly the HOMO and the LUMO energy levels of the silole core (see below and Fig. 13).[48] For **Tp-MPTPS** this transition is slightly red-shifted at 369 nm. This shift could be explained by the stabilization effect of the LUMO induced by the presence of the phenyl group on the silicon atom.[5] The absorption maximum of thin films is
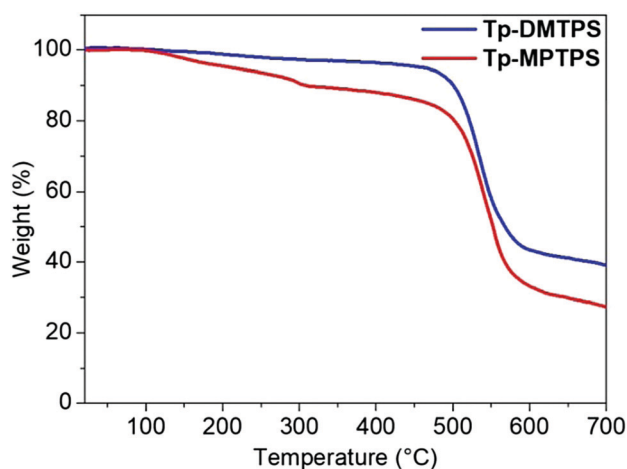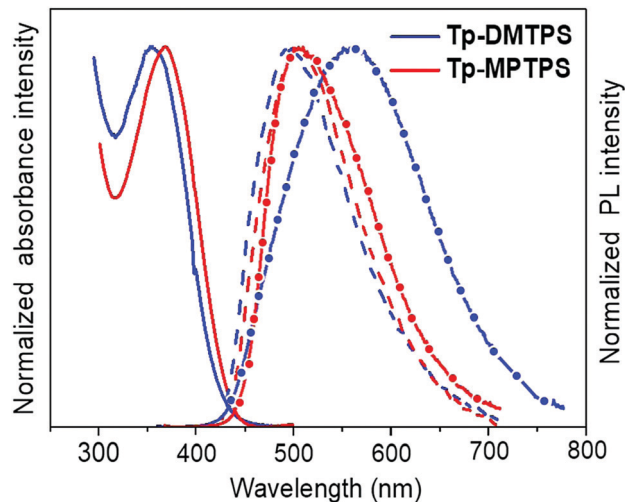

Fig. 7 Absorption (solid lines) and photoluminescence (PL) normalized spectra of **Tp-DMTPS** and **Tp-MPTPS** in CH₂Cl₂ solution (10^{-5} M, dashed lines) and as microcrystalline powders (lines and dotted lines).

slightly red-shifted to 365 nm for **Tp-DMTPS** (Fig. S9, ESI‡), but remains unchanged for **Tp-MPTPS**.

The photoluminescence spectra in solution show faint PL signals with maxima at 486 nm (Φ_f = 1.4%) and 491 nm (Φ_f = 1.2%) for **Tp-DMTPS** and **Tp-MPTPS**, respectively (Fig. 7). In comparison with the corresponding siloles without triptycene, **DMTPS** (λ_{max}^f = 470 nm, Φ_f = 0.2%) and **MPTPS** (λ_{max}^f = 471 nm, Φ_f = 0.1%),[47] **Tp-DMTPS** and **Tp-MPTPS** both shows a small red shift in the emission maxima and a much higher quantum yield.

Since it is known that it is the intramolecular rotation of the phenyl rings in 2,3,4,5-tetraphenylsiloles that makes them essentially non-luminescent when molecularly dissolved,[49] the enhancement of the quantum yields is probably due to the restriction of such intramolecular rotation (RIR) afforded by the triptycene moieties.

In contrast to what is observed in solution, the microcrystalline powders of **Tp-DMTPS** and **Tp-MPTPS** display a rather good fluorescence with emission maxima at 561 and 498 nm, and quantum yields of 43 and 24%, respectively. The same trend is also observed with **DMTPS** and **MPTPS** and was related to the aggregation induced emission (AIE) phenomenon that was reported for the first time with hexaphenylsilole.[50] However, the significant red-shift found in the **Tp-DMTPS** PL spectrum in comparison with what was observed both in solution (λ_{max} = 486 nm) or deposited as 100 nm thick films (λ_{max} = 485 nm, Fig. S10, ESI‡) is surprising.

Aggregation induced emission (AIE)

The AIE properties of **Tp-DMTPS** and **Tp-MPTPS** were studied in THF/water mixtures with different water fractions (f_w) in view of fine-tuning the aggregation extent (Fig. 8). As expected, the larger the water fraction, the stronger the fluorescence; molecular aggregation inducing a red shift of 12 nm in the emission spectrum. As shown in Fig. 8, when f_w varies from 0 to 60 vol%, the fluorescence of **Tp-DMTPS** remains very low. A remarkable 50-fold increase of fluorescence intensity is observed at a water fraction of 90 vol%. The same trend is observed with **Tp-MPTPS**

Fig. 6 TGA plots of **Tp-DMTPS** and **Tp-MPTPS** under nitrogen at a heating rate of 10 °C min⁻¹.

This journal is © The Royal Society of Chemistry and the Chinese Chemical Society 2020

Mater. Chem. Front., 2020, **4**, 2006–2017 | **2009**

Table 2 Optical and electronic properties of **Tp-DMTPS** and **Tp-MPTPS**[a]

	λ_{abs} (nm)		λ_{em} (nm)					
	Soln	Thin film[b]	Soln (Φ_F)	Solid (Φ_F)	E_g^{opt} (eV)	HOMO[c] (eV)	LUMO[c] (eV)	E_g^{el} (eV)
Tp-DMTPS	357	365	486 (1.4)	561 (43)–533 (43)[d]	2.89	−5.54	−2.48	3.06
Tp-MPTPS	369	370	491 (1.2)	498 (24)	2.85	−5.54	−2.51	3.03

[a] λ_{abs} = absorption maximum; λ_{em} = emission maximum; Φ_F = fluorescence quantum yield in CH_2Cl_2 solutions (Soln) and in the solid state (solid); E_g^{opt} = energy gap calculated from the absorption edge; E_g^{el} = electrochemical gap obtained from HOMO and LUMO. [b] 100 nm thick film. [c] HOMO and LUMO levels determined from CVs in CH_2Cl_2/Bu_4NPF_6. [d] First values: microcrystalline powders, second values: ground powders. Excitation wavelength: 365 nm.
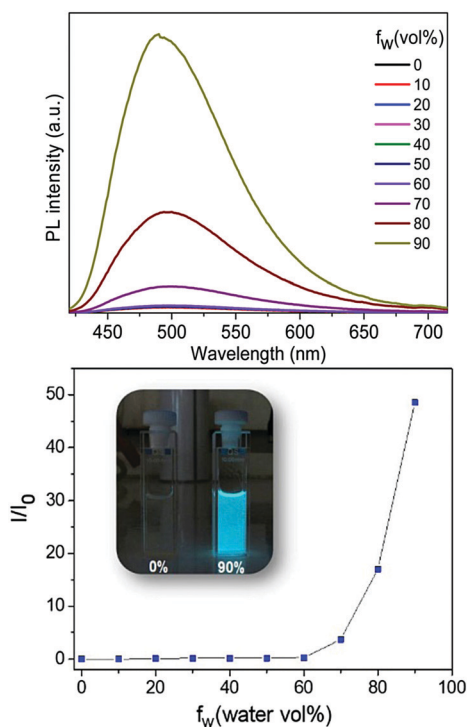

Fig. 8 Top: PL spectra of **Tp-DMTPS** in THF/water mixtures with different water fractions (f_w). Concentration: 10^{-5} M; excitation wavelength: 365 nm. Bottom: Plot of (I/I_0) values *versus* water fractions in THF/water mixtures. I_0 is the PL intensity in pure THF solution. Inset: Photographs **Tp-DMTPS** in THF/water mixtures (f_w = 0 and 90%) taken under UV lamp illumination.

with a 60-fold increase of the fluorescence intensity when f_w also reached 90% (Fig. S12, ESI‡).

Moreover, we found that unlike **Tp-MPTPS**, the position of the emission of **Tp-DMTPS** in the solid state depends strongly on its degree of crystallization. Whereas rapid precipitation of **Tp-DMTPS** by addition of pentane affords a solid exhibiting blue emission under excitation at 365 nm, slow crystallization from acetone/dichloromethane mixtures leads to a yellow-orange emission for the obtained microcrystals (Fig. S11, ESI‡). These changes in emission features should mainly originate from the transition from the crystal to the amorphous state as well as the changes in the molecular conformations.[50–55]

Mechanofluorochromism

The dependence of the position of the **Tp-DMTPS** emission maximum on its procedure of isolation (precipitation/crystallization),
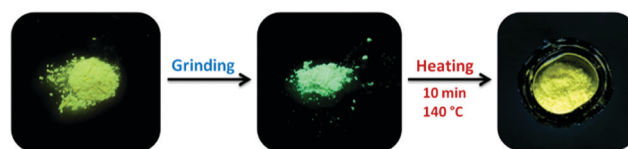

Fig. 9 Photographs of **Tp-DMTPS** under UV illumination before grinding (left), after grinding (middle) and after annealing at 140 °C for 10 min (right).

suggests that this compound could display mechanofluorochromism.[18,56,57] This hypothesis was confirmed by simply grinding a sample of microcrystalline **Tp-DMTPS**. As shown in Fig. 9, the emission turned from orange to blue-green upon UV illumination. It is important to mention that this phenomenon called mechanohypsochromism is rarely observed, a red-shift being observed in almost all cases.[32–37] Finally, the initial orange emission could be restored by heating the ground solid at 140 °C for 10 min. The choice of this annealing temperature was based on the DSC analyses of **Tp-DMTPS** after grinding, which shows an exothermic signal associated to a crystallization process (Fig. S13, ESI‡).

The corresponding PL spectra (Fig. 10) shows that the grinding process is not only affecting the position of the emission maximum (λ_{em}(crystals) = 561 nm, λ_{em}(after grinding) = 533 nm), but is also modifying the peak shape, the solid state quantum yield of emission remaining the same. Interestingly, the emission of the aggregates generated by adding water to a THF solution shows a sharper emission peak (λ_{em} = 498 nm), which is very similar to the one obtained in solution (see Fig. 7). These emission changes should mainly be due to their different molecular conformations that are affected by the crystallinity in these solids.[54,58]
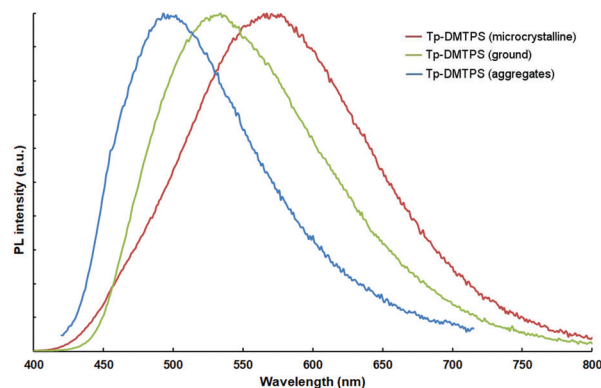

Fig. 10 PL spectra of **Tp-DMTPS** in various forms.

This journal is © The Royal Society of Chemistry and the Chinese Chemical Society 2020

To evaluate the degree of crystallinity, we performed powder XRD analyses, the patterns indicate that grinding microcrystalline **Tp-DMTPS** leads to a dramatic decrease of its crystallinity, but not reaching complete amorphization (Fig. S14, ESI‡). On the other hand, fast precipitation from a mixture of THF with "high" water content should lead to the formation of amorphous aggregates, as previously observed by Tang *et al.*[50,55] Therefore, there is a clear dependency between the long-range molecular order and the emission: the higher the order, the stronger the emission is redshifted. Interestingly, similar experiments conducted with microcrystalline **Tp-MPTPS** powders showed that the position of the emission maximum remains unaffected upon grinding.

Solid state NMR experiments

^{13}C CP-MAS NMR spectra of either microcrystalline or ground powders of **Tp-DMTPS** are shown in Fig. 11. In comparison with the spectrum recorded in CDCl$_3$ solution, the peaks were observed at very similar chemical shifts. The signal arising from the resonance of the methyl groups SI(C1,C1') at $\delta = -3.6$ ppm is split into two, as well as the signals from the carbon atoms belonging to the silole ring SI(C3,C4) $\delta = 154.8$ ppm and SI(C2,C5) $\delta = 141.8$ ppm (see Fig. 1 for labelling). The same splitting is also observed for the carbon atoms PH2(C1) and PH5(C1) ($\delta = 139.0$ ppm), which are directly connected to the silole ring. It is noteworthy that this peak splitting is also noticed, in the ^{13}C CP-MAS NMR spectrum of **DMTPS** but with a smaller extent (Fig. S15, ESI‡). As shown in Fig. 11, grinding the microcrystalline powder does not affect the spectrum pattern to a large extent; only a peak broadening is observed.

These observations are in line with what has been learned from the crystal structure analysis, *i.e.* the splitting of the methyl group signals reflects their non-equivalent environment in the crystal lattice, one being nestled between two phenyl rings. As mentioned above, going from the *R*- to the *L*-conformer brings modifications of the torsion angles φ_2, φ_3, φ_4 and φ_5. Because of them, the conjugation between the surrounding phenyl rings and the silole core should be affected and the resonance peaks corresponding to the carbon atoms involved in the conjugation pathway split into two. This is also what was observed for
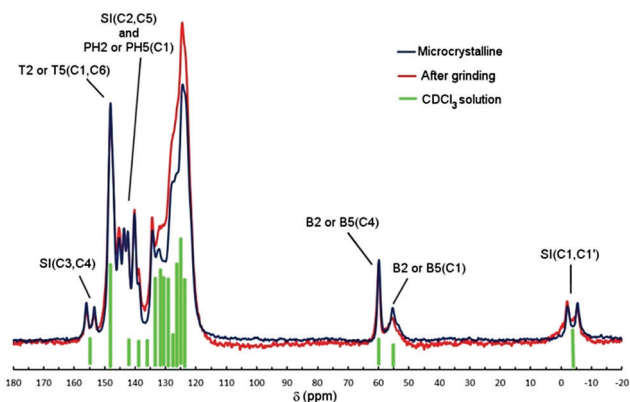
DMTPS, its crystal structure exhibiting two molecules in the asymmetric unit that mainly differ in the rotation of the phenyl groups with respect to the central silole ring.[47]

From the ^{13}C CP-MAS NMR experiments, we have shown that the spectrum of the ground powder is very similar to that of the crystalline one. The only difference consists in the broadening of some resonance peaks that should originate from the loss of crystallinity, as observed by XRD. Therefore, the two methyl groups remaining non-equivalent, this should indicate that a methyl group is always nestled between two phenyl rings both in the crystalline and the ground form. Interestingly, since the emission is blue-shifted, disordering the crystal packing upon grinding appears to favour the emission originating from the less conjugated *L*-conformer. This preference should be due to the stronger CH/π interactions found with this conformer. Finally, when vacuum-deposited as thin films, the PL and EL spectra showed similarities with that measured in solution. This indicates that this deposition process does not promote a good molecular organization even at a very small scale. Contrastingly, **Tp-MPTPS** displayed a more conventional behavior since the conformation of the molecules do not show any noticeable change depending on their physical state as it is observed with its parent **MPTPS**.

Electrochemical properties

Cyclic voltammetry (CV) of **Tp-DMTPS** and **Tp-MPTPS** were recorded in CH$_2$Cl$_2$/Bu$_4$NPF$_6$ (0.2 M) both in oxidation and reduction. In oxidation (Fig. 12, up), both compounds show similar successive oxidation steps with maxima closed to 1.26,
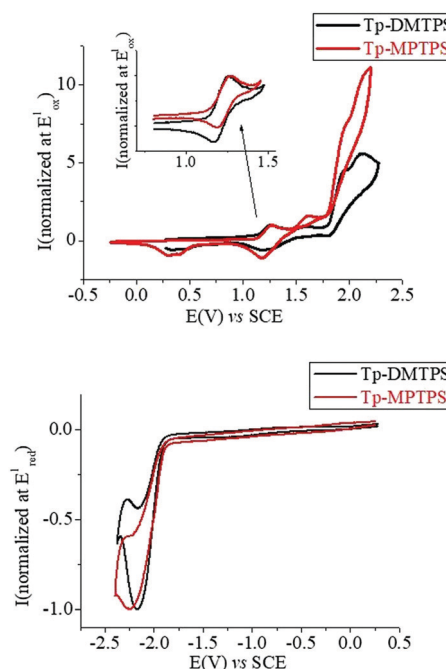

Fig. 12 Top: Cyclic voltammetry in CH$_2$Cl$_2$/Bu$_4$NPF$_6$ (0.2 M) of **Tp-DMTPS** (in black) and **Tp-MPTPS** (in red). Exploration in the anodic direction (top) and in the cathodic direction (bottom). Working electrode: platinum disk, sweep-rate: 100 mV s^{-1}.

Fig. 11 ^{13}C CP-MAS NMR spectra of **Tp-DMTPS** (microcrystalline and ground). Green bars represent the peaks observed in the ^{13}C{^{1}H} NMR spectrum recorded in CDCl$_3$ solution. See Fig. 1 for labelling.

1.60, 1.90 and 2.10 V. Only the first oxidation step is reversible for the two compounds (see inset Fig. 12, top). From the onset potential of this first oxidation (1.14 V for both compounds), the HOMO levels were calculated at −5.54 eV.[59,60] Thus, in the light of theoretical calculation (see further, Fig. 15), this first electron transfer is centered on the phenyl/silole moiety. Recurrent cycles recorded up to the fourth oxidation step, lead for the two compounds to electrodeposition processes with the appearance and growth of new redox systems along the cycles and to the coverage of the electrode surface by insoluble electroactive deposits (Fig. S16 and S17, ESI‡). Although this observation is not directly of interest in the topic of the present work, it is worth mentioning that the deposit obtained from **Tp-MPTPS** present both p- and a n-doping processes with a gap as low as 1.80 eV (see Fig. S17, ESI,‡ right).

As electropolymerization is a useful technique to design low gap materials,[61] the present silole derivatives may be investigated in the future for that purpose. In reduction, both compounds exhibit a similar irreversible reduction wave (Fig. 12, bottom) from which the LUMO levels were calculated around −2.5 eV (−2.48 eV for **Tp-DMTPS** (E_{onset}^{red}: −1.92 V) and −2.51 eV for **Tp-MPTPS** (E_{onset}^{red}: −1.89 V)). The electrochemical gaps (E_g^{el}) for both compounds were calculated to be 3.06 eV for **Tp-DMTPS** and 3.03 eV for **Tp-MPTPS**. These E_g^{el} values and their contraction of 0.03 eV from **Tp-DMTPS** to **Tp-MPTPS** are in accordance with the optical gaps calculated from absorption spectra recorded in CH_2Cl_2 (E_g^{el} = 2.89 eV for **Tp-DMTPS** and 2.85 eV for **Tp-DMTPS**).

Electroluminescence

To evaluate the benefit brought by tritycene groups, we compared **Tp-DMTPS**, **Tp-MPTPS** and **DMTPS** as both emissive and electron transporting layer in OLEDs. Since silole derivatives are good electron transporting materials, particular efforts must be done to have efficient hole injection at the anode for getting high luminescence.[62] Therefore, we have used an ITO/PEDOT–PSS/NPB/silole/Ca simplified architecture to evaluate the performances of these compounds without trying to especially improve them. Because of its tendency to form highly crystalline thin films (Fig. S18, ESI‡), it was very difficult to collect reproducible data from devices made with **DMTPS**. However, we were able to make measurements showing very low performances with a quantum efficiency of 0.08 cd A⁻¹ at 6.0 V (Fig. S19, ESI‡) which is in line with what has been previously described.[63] Contrastingly, **Tp-DMTPS** displays good film-forming ability, the thin films remaining amorphous even after being annealed at 80 °C for 1 h. As seen above, this excellent film stability is due to the drastic enhancement of both thermal and structural properties afforded by the triptycene moieties. Normalized electroluminescence (EL) spectra collected from two different devices are shown in Fig. 13.

The EL spectrum an OLED with the simple architecture ITO/PEDOT–PSS/NPB/**Tp-DMTPS**/Ca displays a maximum at 516 nm, which is not affected by the applied voltage (Fig. S20, ESI‡). The insertion of a MoO_3 layer between PEDOT–PSS and NPB layers (ITO/PEDOT–PSS/MoO_3/NPB/**Tp-DMTPS**/Ca) induces a blue shift of *ca.* 20 nm in the EL spectrum. This could be the consequence
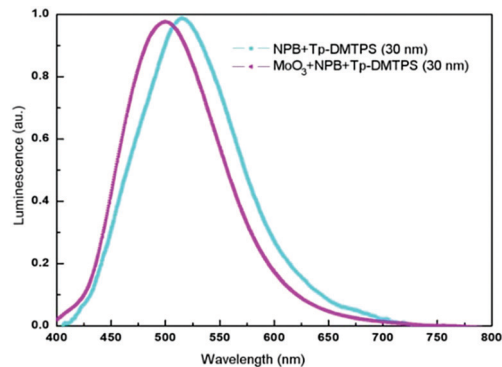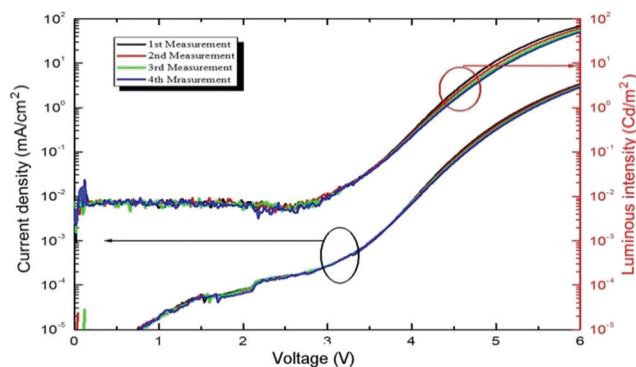

Fig. 13 Normalized EL spectra of **Tp-DMTPS**.

Fig. 14 *J−V* characteristics and luminous intensity *versus* voltage of an ITO/PEDOT–PSS/MoO_3/NPB/**Tp-DMTPS**/Ca device.

of a micro cavity effect, the emission wavelength being affected by the thickness of the active layer.[64]

The current density and luminuous intensity are shown in Fig. 14 for an ITO/PEDOT–PSS/MoO_3/NPB/**Tp-DMTPS**/Ca device. The stability and repeatability for these devices are quite good, the quantum efficiency which is 2.8 cd A⁻¹ at 6.0 V is 35 fold higher than with **DMTPS** and the CIE color coordinates are *x* = 0.228 and *y* = 0.412 (Fig. S21, ESI‡). As anticipated from its lower solid state quantum yield, OLEDs with an ITO/PEDOT–PSS/NPB/**Tp-MPTPS**/Ca architecture show lower performances than those obtained with **Tp-DMTPS**, *i.e.*, 0.8 cd A⁻¹ with CIE color coordinates of *x* = 0.301 and *y* = 0.312 (Fig. S22 and S23, ESI‡).

Electronic structure calculations

The HOMO and LUMO energy levels of both optimized, *R*- and *L*-conformers of **Tp-DMTPS** and **Tp-MPTPS** were estimated at the density functional theory (DFT) level using the B3LYP functional and the 6-31G* basis set. Calculations have been done on single molecules, either fully unconstrained, referred here as "optimized structures" or on structures for which the torsion angles have been frozen to their crystal values during the optimization, noted here as "constrained structures". The optimized structures and the shape of the HOMO and LUMO orbitals of **Tp-DMTPS** and **Tp-MPTPS** are depicted in Fig. 15.

As previously observed, the four phenyl rings decorating the central silole ring adopt a propeller-like arrangement.
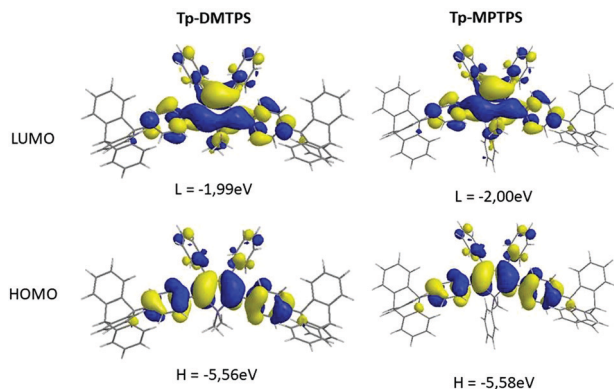
2012 | *Mater. Chem. Front.*, 2020, **4**, 2006–2017

This journal is © The Royal Society of Chemistry and the Chinese Chemical Society 2020

Fig. 15 Energy and shape of the HOMO and LUMO orbitals of optimized structures of **Tp-DMTPS** and **Tp-MPTPS**, as calculated at the B3LYP/6-31+G* level.

Surprisingly, the calculations took rather well into account the strong CH/π interactions found in the crystal structures of both siloles with calculated bending angles of *ca.* 11° (**Tp-DMTPS**) and 15° (**Tp-MPTPS**) between the threefold axis of the triptycene group and the adjacent phenyl moiety. The HOMO orbitals of both derivatives are mainly located on the central silole core and phenyl rings at 2,5-positions while the substituents located at the 3 and 4-positions bear much weaker contributions. Calculated values are −5.56 and −5.58 eV for **Tp-DMTPS** and **Tp-MPTPS**, respectively, values that are close to the ones estimated from CV measurements (see Table 2). This indicates that the optimized structures are certainly close to the ones present in solution. For the LUMO orbitals, a significant σ*-type orbital density is found on the two exocyclic Si–C bonds. This is typical for siloles and the resulting σ(Si–C$_{exocyclic}$)*–π(butadiene)* hyperconjugation is responsible for the stabilization of the LUMO level; making those compounds good candidates for optoelectronic applications.[7] The triptycene moieties are not involved in the frontier orbitals; **Tp-DMTPS** and **Tp-MPTPS** being therefore similar from an electronic point of view to their **DMTPS** and **MPTPS** parents.

Concerning *R*- and *L*-conformers of **Tp-DMTPS** (Fig. 16), as expected from the increased values of the torsion angles with respect to fully optimized structures (Table 1), both conformers
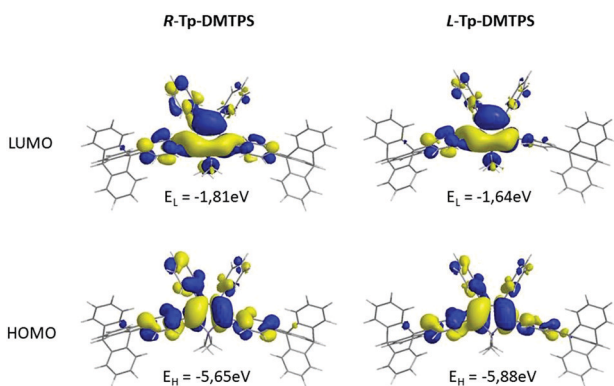
display larger E_g values than for the optimized structure. Indeed, the *L*-conformer that is the less conjugated, displays the largest E_g value of 4.24 eV. Consequently, the emission of **Tp-DMTPS** is expected to be blue-shifted when passing from solution (calculated E_g = 3.37eV) to the solid state, in contrast to experimental observations. This clearly suggests that the red-shift observed experimentally does not stem from the intrinsic properties of the molecules, but rather from the strong CH/π intermolecular interactions that occur in the solid.[65,66]

Charge transport calculations

Finally, we decided to perform quantum-chemical calculation to evaluate both the role the CH/π intermolecular interactions and the conformational modifications in a supramolecular property such as charge transport. Therefore, the estimation of the hole and electron mobilities for both *R*- and *L*-conformers of **Tp-DMTPS** as well as **DMTPS** as a reference were carried out.[67,68] Interestingly, our methodology reproduces nicely the measured electron-transporting character of **DMTPS**[47] with the highest calculated electron mobilities of 0.134 cm² (V s)⁻¹, compared to 0.038 cm² (V s)⁻¹ for holes (see Fig. S24, ESI‡). In contrast to **DMTPS** for which high transport properties are almost isotropic, **Tp-DMTPS** only exhibits a two-dimensional charge transport character within the *bc* plane, especially along the *b* axes. It is worthy to note that this is also in this direction that the main CH/π intermolecular interactions are running (see above). The two-dimensional behavior is a result of the 'insulating character' of the triptycene moiety: since the HOMO and LUMO orbitals are localized on the TPS subunit and not on the triptycene, hole and electron hopping events are highly unlikely along the triptycene direction. Surprisingly, our simulations reveal that, compared to
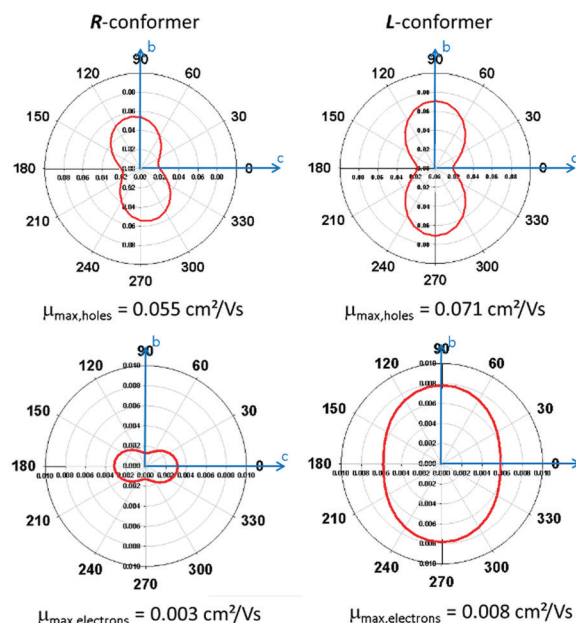

Fig. 17 Anisotropy of the hole (top) and electron (bottom) mobilities (in cm² (V s)⁻¹) in the *R*- (left) and *L*- (right) conformers of **Tp-DMTPS**. The horizontal [vertical] direction corresponds to the *c*-[*b*-] unit cell axis. Note that the mobility scale is different for holes and electrons.

Fig. 16 Energy and shape of the HOMO and LUMO levels of constrained *R*- and *L*-conformers of **Tp-DMTPS** as calculated at the B3LYP/6-31+G* level.

This journal is © The Royal Society of Chemistry and the Chinese Chemical Society 2020

Mater. Chem. Front., 2020, **4**, 2006–2017 | **2013**

DMTPS, hole mobilities are slightly enhanced while electron mobilities are significantly lowered, down to values never exceeding 0.008 cm^2 (V s)$^{-1}$, see Fig. 17. Moreover, an increase of the mobilities is observed when passing from the *R*- to the *L*-conformer of **Tp-DMTPS**. This result is in good agreement with the conclusion drawn by the Hirshfeld surface analysis (see Fig. 5), indicating that the *L*-conformer display stronger CH/π intermolecular interactions than the *R*-conformer. These calculations also show that these interactions are likely involved in the charge transport pathways.

Grafting a triptycene fragment on a TPS central core therefore strongly modifies its charge transport properties by (i) reducing its charge transfer character from 3-D to 2-D and by (ii) inducing a stronger hole-transporting character while keeping a moderate electron mobility. These results imply that **Tp-DMTPS** is able to transport both types of charge carriers reasonably well, consistent with the device performances described above.

Conclusions

Experimental and theoretical studies of two silole–triptycene derivatives **Tp-DMTPS** and **Tp-MPTPS** are presented. Both compounds display a very good AIE activity as well as increased thermal and structural stabilities in comparison with other silole congeners. Consequently, a substantial improvement is found in the formation of stable, amorphous thin films as well as in the performance of simple OLED. Further improvement of the devices performance should be reached through the correction of the charge-transport balance by molecular engineering.[6,69] Among the two molecules, **Tp-DMTPS** displays a very interesting photophysical behavior. In contrast to what is frequently observed, an appreciable red-shift is observed when passing from either the solution or the tiny aggregates to the crystals. Moreover a pronounced reversible mechanohypsochromic phenomenon with a color emission changing from yellow-orange to blue-green is observed when microcrystalline powders are ground. Based on single crystal structural analysis, ^{13}C CP-MAS NMR and theoretical calculations this behavior was rationalized. We have demonstrated the significance of both molecular conformation and intermolecular CH/π interactions. ^{13}C CP-MAS NMR experiments conducted either on microcrystalline or ground powders confirmed that despite of the loss of crystallinity upon grinding, strong intermolecular CH/π interactions are preserved. This reflects the strong structure-directing properties brought by the triptycene groups. The origin of the red-shift observed when passing from isolated molecules to the crystal may be explained by the stabilization of the frontiers energy levels through CH/π intermolecular interactions. On the other hand, the origin of the mechanohypsochromism could be explained by the fact that the more energetic conformer is favored when the crystal environmental strain is diminished. Our results therefore indicate that the attachment of triptycene moieties to π-conjugated molecules is an interesting way to improve their thermal, structural and photophysical properties for sensing or optoelectronic applications. However, further experiments and sophisticated calculations are needed to fully understand this very original behavior.

Conflicts of interest

There are no conflicts to declare.

Acknowledgements

Notes and references

1 J. Dubac, A. Laporterie and G. Manuel, Group 14 metalloles. 1. Synthesis, organic chemistry, and physicochemical data, *Chem. Rev.*, 1990, **90**, 215–263.

2 S. Yamaguchi, R.-Z. Jin, K. Tamao and M. Shiro, Synthesis of a Series of 1,1-Difunctionalized Siloles, *Organometallics*, 1997, **16**, 2230–2232.

3 S. Yamaguchi and K. Tamao, Silole-containing σ- and π-conjugated compounds, *J. Chem. Soc., Dalton Trans.*, 1998, 3693–3702.

4 K. Tamao, M. Uchida, T. Izumizawa, K. Furukawa and S. Yamaguchi, Silole Derivatives as Efficient Electron Transporting Materials, *J. Am. Chem. Soc.*, 1996, **118**, 11974–11975.

5 S. Yamaguchi, T. Endo, M. Uchida, T. Izumizawa, K. Furukawa and K. Tamao, Toward new materials for organic electroluminescent devices: synthesis, structures, and properties of a series of 2,5-diaryl-3,4-diphenylsiloles, *Chem. – Eur. J.*, 2000, **6**, 1683–1692.

6 L. Aubouy, P. Gerbier, N. Huby, G. Wantz, L. Vignau, L. Hirsch and J.-M. Janot, Synthesis of new dipyridylphenyl-aminosiloles for highly emissive organic electroluminescent devices, *New J. Chem.*, 2004, **28**, 1086–1090.

7 Y. Cai, A. Qin and B. Z. Tang, Siloles in optoelectronic devices, *J. Mater. Chem. C*, 2017, **5**, 7375–7389.

8 K. Amro, A. K. Thakur, J. Rault-Berthelot, C. Poriel, L. Hirsch, W. E. Douglas, S. Clement and P. Gerbier, 2,5-Thiophene substituted spirobisiloles – synthesis, characterization, electrochemical properties and performance in bulk heterojunction solar cells, *New J. Chem.*, 2013, **37**, 464–473.

9 J. Luo, Z. Xie, J. W. Y. Lam, L. Cheng, H. Chen, C. Qiu, H. S. Kwok, X. Zhan, Y. Liu, D. Zhu and B. Z. Tang, Aggregation-induced emission of 1-methyl-1,2,3,4,5-pentaphenylsilole, *Chem. Commun.*, 2001, 1740–1741.

10 G. Feng and B. Liu, Aggregation-induced emission (AIE) dots: Emerging theranostic nanolights, *Acc. Chem. Res.*, 2018, **51**, 1404–1414.

2014 | *Mater. Chem. Front.,* 2020, **4**, 2006–2017

This journal is © The Royal Society of Chemistry and the Chinese Chemical Society 2020

11 D. Wang and B. Z. Tang, Aggregation-Induced Emission Luminogens for Activity-Based Sensing, *Acc. Chem. Res.*, 2019, **52**, 2559–2570.

12 Z. Zhao, B. He and B. Z. Tang, Aggregation-induced emission of siloles, *Chem. Sci.*, 2015, **6**, 5347–5365.

13 M. Arribat, E. Remond, S. Richeter, P. Gerbier, S. Clement and F. Cavelier, Silole amino acids with aggregation-induced emission features synthesized by hydrosilylation, *Eur. J. Org. Chem.*, 2019, 2275–2281.

14 J. Mei, N. L. C. Leung, R. T. K. Kwok, J. W. Y. Lam and B. Z. Tang, Aggregation-Induced Emission: Together We Shine, United We Soar!, *Chem. Rev.*, 2015, **115**, 11718–11940.

15 Y. Xie and Z. Li, The development of mechanoluminescence from organic compounds: breakthrough and deep insight, *Mater. Chem. Front.*, 2020, **4**, 317–331.

16 Z. Chi, X. Zhang, B. Xu, X. Zhou, C. Ma, Y. Zhang, S. Liu and J. Xu, Recent advances in organic mechanofluorochromic materials, *Chem. Soc. Rev.*, 2012, **41**, 3878–3896.

17 J.-Y. Zhu, C.-X. Li, P.-Z. Chen, Z. Ma, B. Zou, L.-Y. Niu, G. Cui and Q.-Z. Yang, A polymorphic fluorescent material with strong solid state emission and multi-stimuli-responsive properties, *Mater. Chem. Front.*, 2020, **4**, 176–181.

18 L. Wilbraham, M. Louis, D. Alberga, A. Brosseau, R. Guillot, F. Ito, F. Labat, R. Metivier, C. Allain and I. Ciofini, Revealing the Origins of Mechanically Induced Fluorescence Changes in Organic Molecular Crystals, *Adv. Mater.*, 2018, **30**, 1800817.

19 X. Luo, J. Li, C. Li, L. Heng, Y. Q. Dong, Z. Liu, Z. Bo and B. Z. Tang, Reversible Switching of the Emission of Diphenyldibenzofulvenes by Thermal and Mechanical Stimuli, *Adv. Mater.*, 2011, **23**, 3261–3265.

20 N. Zhao, Z. Yang, J. W. Y. Lam, H. H. Y. Sung, N. Xie, S. Chen, H. Su, M. Gao, I. D. Williams, K. S. Wong and B. Z. Tang, Benzothiazolium-functionalized tetraphenylethene: an AIE luminogen with tunable solid-state emission, *Chem. Commun.*, 2012, **48**, 8637–8639.

21 K. Walzer, B. Maennig, M. Pfeiffer and K. Leo, Highly Efficient Organic Devices Based on Electrically Doped Transport Layers, *Chem. Rev.*, 2007, **107**, 1233–1271.

22 P. Kordt, J. J. M. van der Holst, M. Al Helwi, W. Kowalsky, F. May, A. Badinski, C. Lennartz and D. Andrienko, Modeling of Organic Light Emitting Diodes: From Molecular to Device Properties, *Adv. Funct. Mater.*, 2015, **25**, 1955–1971.

23 X. Zhou, J. He, L. S. Liao, M. Lu, X. M. Ding, X. Y. Hou, X. M. Zhang, X. Q. He and S. T. Lee, Real-time observation of temperature rise and thermal breakdown processes in organic LEDs using an IR imaging and analysis system, *Adv. Mater.*, 2000, **12**, 265–269.

24 G. Wantz, L. Derue, O. Dautel, A. Rivaton, P. Hudhomme and C. Dagron-Lartigau, Stabilizing polymer-based bulk heterojunction solar cells via crosslinking, *Polym. Int.*, 2014, **63**, 1346–1361.

25 T. M. Swager, Iptycenes in the Design of High Performance Polymers, *Acc. Chem. Res.*, 2008, **41**, 1181–1189.

26 J. H. Chong and M. J. MacLachlan, Iptycenes in supramolecular and materials chemistry, *Chem. Soc. Rev.*, 2009, **38**, 3301–3315.

27 Y. Jiang and C.-F. Chen, Recent Developments in Synthesis and Applications of Triptycene and Pentiptycene Derivatives, *Eur. J. Org. Chem.*, 2011, 6377–6403.

28 G. M. Locke, S. S. R. Bernhard and M. O. Senge, Nonconjugated Hydrocarbons as Rigid-Linear Motifs: Isosteres for Material Sciences and Bioorganic and Medicinal Chemistry, *Chem. – Eur. J.*, 2019, **25**, 4590–4647.

29 H.-H. Chou, H.-H. Shih and C.-H. Cheng, Triptycene derivatives as high-T_g host materials for various electrophosphorescent devices, *J. Mater. Chem.*, 2010, **20**, 798–805.

30 S. Jhulki, T. J. Chow and J. N. Moorthy, Benzophenone-imbedded benzoyltriptycene with high triplet energy for application as a universal host material in phosphorescent organic light-emitting diodes (PhOLEDs), *New J. Chem.*, 2016, **40**, 6854–6859.

31 Y. Wang, Y.-P. Xiao, Y.-Y. Zhou, C.-G. Hu, B.-H. Tong, S.-H. Ye and Q.-B. Mei, Novel phosphorescent triptycene-based Ir(III) complexes for organic light-emitting diodes, *Dalton Trans.*, 2019, **48**, 16289–16297.

32 K. Nagura, S. Saito, H. Yusa, H. Yamawaki, H. Fujihisa, H. Sato, Y. Shimoikeda and S. Yamaguchi, Distinct Responses to Mechanical Grinding and Hydrostatic Pressure in Luminescent Chromism of Tetrathiazolylthiophene, *J. Am. Chem. Soc.*, 2013, **135**, 10322–10325.

33 M. Tanioka, S. Kamino, A. Muranaka, Y. Ooyama, H. Ota, Y. Shirasaki, J. Horigome, M. Ueda, M. Uchiyama, D. Sawada and S. Enomoto, Reversible Near-Infrared/Blue Mechanofluorochromism of Aminobenzopyranoxanthene, *J. Am. Chem. Soc.*, 2015, **137**, 6436–6439.

34 L. Wang, K. Wang, B. Zou, K. Ye, H. Zhang and Y. Wang, Luminescent Chromism of Boron Diketonate Crystals: Distinct Responses to Different Stresses, *Adv. Mater.*, 2015, **27**, 2918–2922.

35 J. Wu, Y. Cheng, J. Lan, D. Wu, S. Qian, L. Yan, Z. He, X. Li, K. Wang, B. Zou and J. You, Molecular Engineering of Mechanochromic Materials by Programmed C-H Arylation: Making a Counterpoint in the Chromism Trend, *J. Am. Chem. Soc.*, 2016, **138**, 12803–12812.

36 S. Ying, M. Chen, Z. Liu, M. Zheng, H. Zhang, S. Xue and W. Yang, Unusual mechanohypsochromic luminescence and unique bidirectional thermofluorochromism of long-alkylated simple DPP dyes, *J. Mater. Chem. C*, 2017, **5**, 5994–5998.

37 K. Zhang, Z. Zhang, X. Fan, L. Tang, Q. Ding, K. Yang, M. Zhai, H. Zhang, S. Xue and W. Yang, Enabling DPP derivatives to show multistate emission and developing the multifunctional materials by rational branching effect, *Dyes Pigm.*, 2018, **159**, 290–297.

38 M. Uchida, T. Izumizawa, T. Nakano, S. Yamaguchi, K. Tamao and K. Furukawa, Structural Optimization of 2,5-Diarylsiloles as Excellent Electron-Transporting Materials for Organic Electroluminescent Devices, *Chem. Mater.*, 2001, **13**, 2680–2683.

39 S. Murphy, X. Yang and G. B. Schuster, Cyanine Borate Salts that Form Penetrated Ion Pairs in Benzene Solution: Synthesis, Properties, and Structure, *J. Org. Chem.*, 1995, **60**, 2411–2422.

This journal is © The Royal Society of Chemistry and the Chinese Chemical Society 2020

Mater. Chem. Front., 2020, **4**, 2006–2017 | **2015**

40 M. Nishio, The CH/π hydrogen bond in chemistry. Conformation, supramolecules, optical resolution and interactions involving carbohydrates, *Phys. Chem. Chem. Phys.*, 2011, **13**, 13873–13900.

41 K. Nikitin, C. Fleming, H. Mueller-Bunz, Y. Ortin and M. J. McGlinchey, Severe Energy Costs of Double Steric Interactions: towards a Molecular Clamp, *Eur. J. Org. Chem.*, 2010, 5203–5216.

42 L. J. Sicard, H.-C. Li, Q. Wang, X.-Y. Liu, O. Jeannin, J. Rault-Berthelot, L.-S. Liao, Z.-Q. Jiang and C. Poriel, C1-Linked Spirobifluorene Dimers: Pure Hydrocarbon Hosts for High-Performance Blue Phosphorescent OLEDs, *Angew. Chem., Int. Ed.*, 2019, **58**, 3848–3853.

43 Y. N. Imai, Y. Inoue, I. Nakanishi and K. Kitaura, Cl-π interactions in protein-ligand complexes, *Protein Sci.*, 2008, **17**, 1129–1137.

44 M. A. Spackman and P. G. Byrom, A novel definition of a molecule in a crystal, *Chem. Phys. Lett.*, 1997, **267**, 215–220.

45 S. K. Wolff, D. J. Grimwood, J. J. McKinnon, M. J. Turner, D. Jayatilaka and M. A. Spackmann, *CrystalExplorer*, University of Western Australia, 2012.

46 J. J. McKinnon, D. Jayatilaka and M. A. Spackman, Towards quantitative analysis of intermolecular interactions with Hirshfeld surfaces, *Chem. Commun.*, 2007, 3814–3816.

47 G. Yu, S. Yin, Y. Liu, J. Chen, X. Xu, X. Sun, D. Ma, X. Zhan, Q. Peng, Z. Shuai, B. Tang, D. Zhu, W. Fang and Y. Luo, Structures, Electronic States, Photoluminescence, and Carrier Transport Properties of 1,1-Disubstituted 2,3,4,5-Tetraphenyl-siloles, *J. Am. Chem. Soc.*, 2005, **127**, 6335–6346.

48 S. Yamaguchi and K. Tamao, Silole-containing π-conjugated polymers. 5. Theoretical study of the electronic structure of 2,2′-bisilole in comparison with 1,1′-bi-1,3-cyclopentadiene: σ*-π* conjugation and a low-lying LUMO as the origin of the unusual optical properties of 3,3′,4,4′-tetraphenyl-2,2′-bisilole, *Bull. Chem. Soc. Jpn.*, 1996, **69**, 2327–2334.

49 J. Chen, C. C. W. Law, J. W. Y. Lam, Y. Dong, S. M. F. Lo, I. D. Williams, D. Zhu and B. Z. Tang, Synthesis, Light Emission, Nanoaggregation, and Restricted Intramolecular Rotation of 1,1-Substituted 2,3,4,5-Tetraphenylsiloles, *Chem. Mater.*, 2003, **15**, 1535–1546.

50 Y. Hong, J. W. Y. Lam and B. Z. Tang, Aggregation-induced emission: phenomenon, mechanism and applications, *Chem. Commun.*, 2009, 4332–4353.

51 R. Cao, L. Ai, H. Yang, S. Li and C. Xu, Aggregation-tuned dual emission of silole derivatives: synthesis, crystal structure, and photophysical properties, *New J. Chem.*, 2020, **44**, 5049–5055.

52 L. Heng, J. Zhai, A. Qin, Y. Zhang, Y. Dong, B. Z. Tang and L. Jiang, Fabrication of hexaphenylsilole nanowires and their morphology-tunable photoluminescence, *ChemPhysChem*, 2007, **8**, 1513–1518.

53 J. Yang, N. Sun, J. Huang, Q. Li, Q. Peng, X. Tang, Y. Dong, D. Ma and Z. Li, New AIEgens containing tetraphenylethene and silole moieties: tunable intramolecular conjugation, aggregation-induced emission characteristics and good device performance, *J. Mater. Chem. C*, 2015, **3**, 2624–2631.

54 C. Wang, B. Xu, M. Li, Z. Chi, Y. Xie, Q. Li and Z. Li, A stable tetraphenylethene derivative: aggregation-induced emission, different crystalline polymorphs, and totally different mechanoluminescence properties, *Mater. Horiz.*, 2016, **3**, 220–225.

55 Y. Dong, J. W. Y. Lam, Z. Li, A. Qin, H. Tong, Y. Dong, X. Feng and B. Z. Tang, Vapochromism of Hexaphenylsilole, *J. Inorg. Organomet. Polym. Mater.*, 2005, **15**, 287–291.

56 T. Mutai, H. Tomoda, T. Ohkawa, Y. Yabe and K. Araki, Switching of polymorph-dependent ESIPT luminescence of an imidazo[1,2-a]pyridine derivative, *Angew. Chem., Int. Ed.*, 2008, **47**, 9522–9524.

57 Y. Sagara and T. Kato, Mechanically induced luminescence changes in molecular assemblies, *Nat. Chem.*, 2009, **1**, 605–610.

58 J. Yang, Z. Ren, B. Chen, M. Fang, Z. Zhao, B. Z. Tang, Q. Peng and Z. Li, Three polymorphs of one luminogen: how the molecular packing affects the RTP and AIE properties?, *J. Mater. Chem. C*, 2017, **5**, 9242–9246.

59 A. P. Kulkarni, C. J. Tonzola, A. Babel and S. A. Jenekhe, Electron Transport Materials for Organic Light-Emitting Diodes, *Chem. Mater.*, 2004, **16**, 4556–4573.

60 C. M. Cardona, W. Li, A. E. Kaifer, D. Stockdale and G. C. Bazan, Electrochemical Considerations for Determining Absolute Frontier Orbital Energy Levels of Conjugated Polymers for Solar Cell Applications, *Adv. Mater.*, 2011, **23**, 2367–2371.

61 C. Paul-Roth, J. Rault-Berthelot, G. Simonneaux, C. Poriel, M. Abdalilah and J. Letessier, Electroactive films of poly-(tetraphenylporphyrins) with reduced bandgap, *J. Electroanal. Chem.*, 2006, **597**, 19–27.

62 N. Huby, L. Hirsch, G. Wantz, L. Vignau, A. S. Barriere, J. P. Parneix, L. Aubouy and P. Gerbier, Injection and transport processes in organic light emitting diodes based on a silole derivative, *J. Appl. Phys.*, 2006, **99**, 084907.

63 B. Z. Tang, X. Zhan, G. Yu, P. P. S. Lee, Y. Liu and D. Zhu, Efficient blue emission from siloles, *J. Mater. Chem.*, 2001, **11**, 2974–2978.

64 A. Dodabalapur, L. J. Rothberg, T. M. Miller and E. W. Kwock, Microcavity effects in organic semiconductors, *Appl. Phys. Lett.*, 1994, **64**, 2486–2488.

65 N. Huby, L. Hirsch, L. Aubouy, P. Gerbier, A. Van Der Lee, F. Amy and A. Kahn, Evidence of environmental strains on charge injection in silole-based organic light-emitting diodes, *Phys. Rev. B: Condens. Matter Mater. Phys.*, 2007, **75**, 115416.

66 D. Kokkin, M. Ivanov, J. Loman, J.-Z. Cai, B. Uhler, N. Reilly, R. Rathore and S. A. Reid, π–π stacking *vs.* C–H/π interaction: Excimer formation and charge resonance stabilization in van der Waals clusters of 9,9′-dimethylfluorene, *J. Chem. Phys.*, 2018, **149**, 134314.

67 C. Niebel, Y. Kim, C. Ruzie, J. Karpinska, B. Chattopadhyay, G. Schweicher, A. Richard, V. Lemaur, Y. Olivier, J. Cornil, A. R. Kennedy, Y. Diao, W.-Y. Lee, S. Mannsfeld, Z. Bao and Y. H. Geerts, Thienoacene dimers based on the thieno[3,2-b]thiophene moiety: synthesis, characterization

2016 | *Mater. Chem. Front.*, 2020, **4**, 2006–2017

This journal is © The Royal Society of Chemistry and the Chinese Chemical Society 2020

and electronic properties, *J. Mater. Chem. C*, 2015, **3**, 674–685.

68 G. Schweicher, V. Lemaur, C. Niebel, C. Ruzie, Y. Diao, O. Goto, W.-Y. Lee, Y. Kim, J.-B. Arlin, J. Karpinska, A. R. Kennedy, S. R. Parkin, Y. Olivier, S. C. B. Mannsfeld, J. Cornil, Y. H. Geerts and Z. Bao, Bulky end-capped [1]benzothieno[3,2-b]benzothiophenes: Reaching high-mobility organic semiconductors by fine tuning of the crystalline solid-state order, *Adv. Mater.*, 2015, **27**, 3066–3072.

69 L. Chen, Y. Jiang, H. Nie, P. Lu, H. H. Y. Sung, I. D. Williams, H. S. Kwok, F. Huang, A. Qin, Z. Zhao and B. Z. Tang, Creation of Bifunctional Materials: Improve Electron-Transporting Ability of Light Emitters Based on AIE-Active 2,3,4,5-Tetraphenylsiloles, *Adv. Funct. Mater.*, 2014, **24**, 3621–3630.